Reaction-Path Dynamics of Hydroxyl Radical Reactions with Ethane and Haloethanes

Sanja Sekušak,[†] Klaus R. Liedl,[‡] Bernd M. Rode,[‡] and Aleksandar Sabljić*[,†,§]

Institute Ruđer Bošković, Department of Chemistry, P.O.B. 1016, HR-10001 Zagreb, Republic of Croatia, Institute of General, Inorganic and Theoretical Chemistry, University of Innsbruck, Innrain 52a, A-6020 Innsbruck, Austria, and Institut für Meteorologie und Klimaforschung, Forschungszentrum Karlsruhe/ Universität Karlsruhe, D-76021 Karlsruhe, Germany

Received: December 6, 1996; In Final Form: March 28, 1997[⊗]

A detailed analysis of reaction-path dynamics of hydrogen abstraction from ethane, fluoroethane, and chloroethane by hydroxyl radical has been performed by the variational transition-state theory augmented with multidimensional semiclassical tunneling approximations. The minimum energy path and its first and second derivatives were calculated at the MP2(full)/6-31G(d,p) level of theory. The calculated barrier heights were further improved by Gaussian-2(MP2) methodology. This dual-level dynamic approach has been used to calculate the reaction rate constants for temperatures from 200 to 1000 K. The contribution from tunneling effect was evaluated using the semiclassical zero-curvature and small-curvature tunneling approximations. The calculated thermal reaction rate constants agree well with the experimental results. The variational effects on the location of central dynamical bottleneck are significant for all three reactions. The competition between potential and vibrational energies in determining the location of the variational transition-state shifts the dynamical bottleneck toward reactants. The influence of halogen substitution on the reaction rate constant is also discussed.

Introduction

Reactions of hydroxyl (OH) radical with hydrocarbons and their halogenated derivatives play an important role in combustion chemistry and in the chemistry of the atmosphere.[1] The release of chlorofluorocarbons (CFCs) into the atmosphere has adverse environmental effect, i.e., the depletion of the ozone layer and the creation of ozone holes.[2,3] Thus, an international effort is underway to phase out CFCs soon and to replace them with environmentally acceptable alternatives.[3,4] Various hydrofluorocarbons (HFCs) are under consideration as a viable CFCs replacements.[4c,d] They have two important advantages that make them environmentally far more acceptable. HFCs contain no chlorine atoms that will participate in the destruction of ozone molecules and have considerably shorter tropospheric lifetimes[1] due to the possible hydrogen abstraction reaction by OH radicals in the lower atmosphere.

Since reactivity with OH radicals is the rate-determining step for the tropospheric lifetimes of all partially halogenated hydrocarbons (HFCs and HCFCs), this reaction has attracted considerable attention of experimentalists[1,2] and theoreticians.[5−8] Efforts have been focused on studying the structures, energetics, and vibrational frequencies of the reactants, products, and transition-state structures for hydroxyl radical reactions with the two simplest hydrocarbons, methane[5a−e,6a,b] and ethane[6c,7a,8a] and their halogenated analogues.[5j,7b,8] However, theoretical studies on the kinetics of these reactions have been limited.[6,7a] Only methane[6a,b] and ethane[6c] reactions with OH radical have been studied in terms of interpolated variational transition-state theory (IVTST)[9] with small curvature tunneling (SCT) corrections.[10] The first- or second-order IVTST is based only on the electronic structure calculations for reactants, products, transition-state structures, and one or two additional points displaced by a small distance from the saddle point.

The aim of this study is to investigate in detail the reaction-path dynamics of ethane and haloethane reactions with OH radical and the role of halogen substitution on the reactivity of haloethanes in hydrogen abstraction reaction. It is well-known that the hydroxyl radical reacts with alkanes and haloalkanes by preferentially abstracting hydrogen atoms from the sites with lower bond energies.[1] Thus, only the kinetics of α-abstraction, i.e., reactions (R1)−(R3), has been investigated in this study.

$$CH_3CH_3 + OH^\bullet \rightarrow CH_3CH_2^\bullet + H_2O \qquad (R1)$$

$$CH_3CH_2F + OH^\bullet \rightarrow CH_3CHF^\bullet + H_2O \qquad (R2)$$

$$CH_3CH_2Cl + OH^\bullet \rightarrow CH_3CHCl^\bullet + H_2O \qquad (R3)$$

A detailed analysis of the minimum energy path (MEP), calculated by molecular quantum mechanical methods with proper inclusion of electron correlation, has been performed for these three hydrogen abstraction reactions. Their reaction rate constants have been calculated for a wide temperature range by the application of dual-level dynamics[11] based on the variational transition-state theory[12,13] (VTST) and on semiclassical tunneling methods[13] and compared with available experimental results. Finally, the reactivity trends along the series of studied compounds have been analyzed and discussed.

Methods

Electronic Structure Calculations. The geometries of all stationary points along the reaction path were optimized and their vibrational frequencies were calculated using second-order Møller−Plesset perturbation theory (MP2)[14] with the 6-31G-(d,p) basis set.[15] The minimum energy path (MEP) was calculated for all three reactions using the Gonzalez−Schlegel IRC algorithm[16] at the same level of theory. The accurate energies of the reactants, transition-state structures, and products

* Corresponding author. Phone (385-1) 456-1089; Fax (385-1) 272-648; E-mail:sabljic@olimp.irb.hr.
† Institute Ruđer Bošković.
‡ University of Innsbruck.
§ Institut für Meteorologie und Klimaforschung.
⊗ Abstract published in *Advance ACS Abstracts,* May 15, 1997.

S1089-5639(96)04006-6 CCC: $14.00

were also calculated using the G2(MP2)[17,18] scheme, and these values were used to correct the MP2/6-31G(d,p) reaction path for the IVTST-IC reaction rate calculations.[9b] Our G2 results published previously[8] for the fluoroethane reaction with OH radical were used to evaluate G2(MP2) results from this study. For the open-shell systems Schlegel's spin projection scheme[19] was used to eliminate spin contamination arising from states with spin $(S + 1)$ to $(S + 4)$. Electronic structure calculations were done using the GAUSSIAN 92 and 94 quantum mechanical packages.[20]

Reaction Rate Calculations. The reaction rate constants were calculated using both conventional (TST)[21] and variational (VTST)[11,13,22,23] transition-state theory. VTST calculations are based on the application of canonical variational theory (CVT).[11,22,24] Furthermore, an interpolation using a modest number of high-level points along the MEP (about 20) was used to calculate the reaction rate constants. We will call this approach the interpolated variational transition-state theory (IVTST). As a final step this approach was refined by using interpolated corrections[9b] of the barrier height at the G2(MP2) level of theory, and the complete procedure will designated as IVTST-IC or G2(MP2)///MP2/6-31G(d,p). It should be noticed that this approach is different from the IVTST of Truhlar et al.,[9a] where only four or five high-level points are used to interpolate all other information needed for VTST.

The IVTST-IC procedure was performed in two steps. First, reaction path calculations were performed for reactions R1, R2, and R3. That is, the minimum energy paths were calculated at the MP2/6-31G(d,p) level of theory, and the gradients and force constant matrixes were evaluated at the same level. Then, the results of energy calculations at the G2(MP2) level of theory were used to interpolate corrections to the energies obtained at the lower level of theory. For all reaction-path calculations we used mass-scaled coordinates with a scaling mass of 1 amu.

A cubic spline interpolation for the energy and the frequencies was implemented in the POLYRATE version 6.5[25] program in order to obtain smooth interpolated values for both quantities.[26] Results obtained with the cubic spline interpolation are comparable with those obtained by using three-point Lagrangian interpolation originally implemented in the POLYRATE version 6.5 program.

The harmonic approximation is assumed for the calculation of vibrational partition functions in all cases except for the internal hindered-rotation of the OH group around the reactive $O-H_a$ bond at the transition state and along the MEP, where a hindered rotor[27] model has been employed.

Because transfer of a hydrogen atom is involved in these reactions, tunneling effects have been approximated by using zero[28,29] and small[29,30] curvature correction methods (ZCT and SCT). The Wigner correction[31] was also calculated because it is the simplest and one of the most commonly used methods for approximating reaction-coordinate tunneling in conventional TST.

The IVTST-IC reaction rate constant calculations were carried out with POLYRATE version 6.5[25] program. Results of VTST-IC and related approaches[11,12,22,23] have been compared with experiments[6,32,33] and accurate quantum dynamics calculations[23,24] with appreciable success; thus, these methods provide reasonably convenient means for solving theoretically kinetic problems of chemically interesting systems.

Experimental Results. The reaction of ethane with OH radical has been studied by several experimental techniques, yielding the reaction rate constants for a wide range of temperatures.[1,35] On the contrary, there is only a few measurements[1d,36,37] from which the reaction rate constants are determined for the reactions of fluoro- and chloroethanes with OH radical. From their temperature dependence, Arrhenius activation energies (E_a) have been obtained. For reaction R1 the range of E_a is 2.1−2.3 kcal mol^{-1}, for R2 1.5−2.3 kcal mol^{-1}, and for R3 0.8−2.0 kcal mol^{-1}.

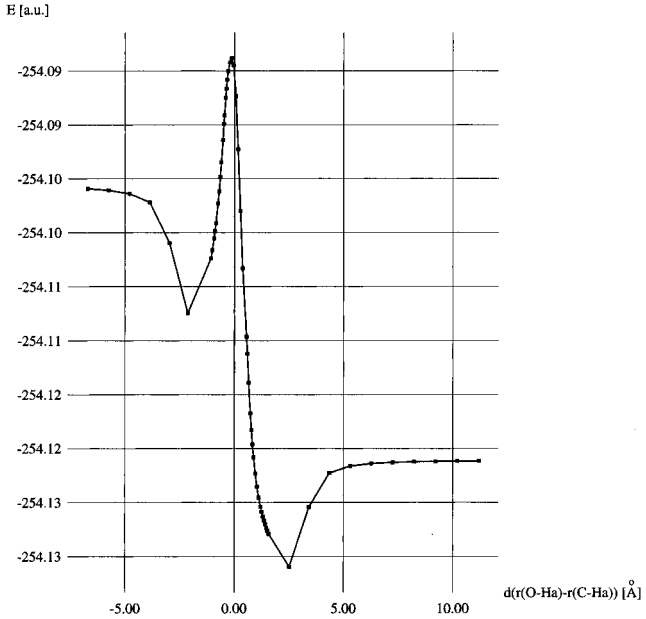

Figure 1. Minimum energy path for the fluoroethane reaction with hydroxyl radical.

Comparison of Experimental and Calculated Reaction Barriers. The comparison of calculated reaction barriers with those obtained from experiments is not a straightforward procedure. Calculated barriers can be expressed as the difference between transition-state and reactants potential energies (V_B) or potential energies corrected for zero-point energies ($\Delta E_0^{\ddagger}$). Adding thermal corrections to $\Delta E_0^{\ddagger}$, $\Delta E_T^{\ddagger}$ is obtained. It is regularly assumed that the Arrhenius activation energy, E_A, can be obtained by adding an RT term to $\Delta E_T^{\ddagger}$.[38] However, this is true only for a restricted class of reactions that follow activated-complex theory with the simplest assumptions about the temperature dependence of the partition coefficients and with temperature-independent transmission coefficients (κ). This is not the case if tunneling is important.[39] However, it was shown recently that, for proton-transfer reactions, a comparison of E_a with $\Delta E_0^{\ddagger}$ is at least an reasonable approximation.[7a]

Results and Discussion

Stationary Points Energetics. The potential energy change along the reaction path of fluoroethane reaction with OH radical with respect to the difference between two reactive bonds, $r(C-H_a)$ and $r(O-H_a)$ is given in Figure 1. Five stationary points were found along the hydrogen abstraction reaction path: reactants, reactant complex, transition-state structure, product complex, and products. Our previous studies[8] report in detail ab initio calculations for the reactants, products and transition-state structures of reactions R1, R2, and R3. Here, we will briefly discuss the electronic structure results for complexes and focus our attention on the reaction dynamics.

Structures of the van der Waals complexes on the reactant and products side of the MEP (C_R, C_P) are calculated for the first time and results are given in Figure 2. The C_R and C_P structures are very similar to separate reactant and product species, respectively. Energy differences between reactants, reactant complexes, transition-state structures, product complexes, and products calculated at the MP2/6-31G(d,p) level of theory for reactions R1, R2, and R3 are given in Table 1.

The reactant and product complexes are formed without barrier from the reactant and product species, respectively. van

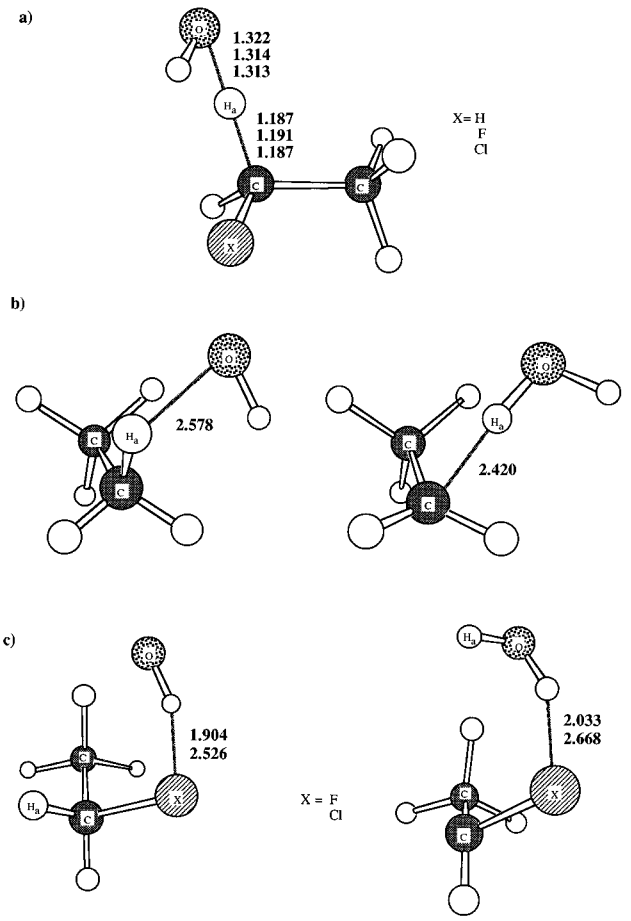

Figure 2. Reactive geometry parameters for (a) transition-state structures, (b) van der Waals complex structures for ethane reaction with OH radical, and (c) van der Waals complex structures for fluoroethane and chloroethane reactions with OH radical calculated at the MP2/6-31G(d,p) level of theory.

TABLE 1: Energy Differences between Reactants, Reactant Complex, Transition-State Structure, Product Complex, and Products along the Minimum Energy Path Calculated at MP2/6-31G(d,p) Level of Theory (All Values Corrected for the Zero-Point Energies and Reported in kcal mol^{-1})

reaction[a]	ΔE_1	ΔE_2	ΔE_3	ΔE_4	$\Delta E^{\ddagger}$	ΔH_r
$C_2H_6 + OH$	−0.6	6.1	−20.4	−1.4	5.5	−15.3
$C_2H_5F + OH$	−5.4	9.3	−25.2	−4.2	3.9	−17.0
$C_2H_5Cl + OH$	−3.1	7.2	−25.0	−2.7	4.1	−18.1

[a] Reactants $\xrightarrow{\Delta E_1}$ complex-R $\xrightarrow{\Delta E_2}$ TS $\xrightarrow{\Delta E_3}$ complex-P $\xrightarrow{\Delta E_4}$ products

der Waals complexes formed in the haloethanes reactions with OH radical are quite different from those formed in the ethane reaction with OH radical. Structures of the van der Waals complexes formed in the reaction of ethane with OH radical are similar to the transition-state structure, the major difference being in the reactive O···H_a···C distances. In the case of haloethanes, both C_R and C_P are characterized by the interaction between halogen atom and hydrogen from OH radical or water molecule, respectively. In terms of natural bond orbital analysis,[40] this interaction can be described as delocalization of the halogen lone-pair electrons into the σ^*(OH) antibonding orbital of the hydroxyl radical or water molecule, respectively.

Accurate energies calculated at the G2(MP2) level of theory for reactants, products and transition states, were used for interpolated corrections, despite the fact that reactant and product complexes are lower in energy than the reactants and products. In all three reactions, we were able to calculate the MEP all the way down to the complexes valley on the product side of the MEP but not on the reactant side due to the convergence problems of the IRC algorithm. The product complexes were found at $s = 5.4$ au for reaction R1, at $s = 8.8$ au for reaction R2, and at $s = 11.0$ au for reaction R3.

TABLE 2: Comparison of Reaction Barriers ($\Delta E_0^{\ddagger}$) Calculated at the G2(MP2) Level of Theory and Arrhenius Activation Energies (E_a) Obtained from the Experimental Reaction Rate Constants (Results in kcal mol^{-1})

reactant	$\Delta E_0^{\ddagger}$	E_a
ethane	2.9	2.1−2.3[a]
fluoroethane	2.1	1.5−2.3[b]
chloroethane	1.1	0.8−2.0[c]

[a] References 1 and 35. [b] Reference 36. [c] References 1d and 37.

The reaction barrier heights for ethane, fluoroethane, and chloroethane reactions with OH radical calculated at the G2(MP2) are given in Table 2. The quality of G2(MP2) results was tested for the fluoroethane reaction with OH radical by comparing its results with G2 results. The barrier height ($\Delta E_0^{\ddagger}$) calculated at the G2 level[8b,c] is 2.09 kcal mol^{-1} which is very close to the G2(MP2) value of 2.10 kcal mol^{-1}. The G2(MP2) results of similar quality are expected for reactions R1 and R3.

Analysis of Reaction Path Properties. Information on geometries and frequencies of the reactants and transition-state structures, the reduced moment of inertia for the internal rotational mode of the transition state, and the energy difference between transition state and reactants are sufficient for the calculation of reaction rate constants by conventional transition-state theory. However, additional information along the minimum energy path is needed for variationally maximizing the generalized free energy as required by VTST. Therefore, the minimum energy paths for the ethane, fluoroethane and chloroethane reactions with OH radical were computed at the MP2/6-31G(d,p) level in steps of 0.1 au. Figure 3 shows the Born−Oppenheimer energy along the minimum energy path ($V_{MEP}(s)$) and the vibrationally adiabatic ground-state potential energy curve ($V_a^G(s)$) for reactions R1, R2, and R3.

The most pronounced changes of reactive geometrical parameters r(C−H_a) and r(O−H_a) occur in the vicinity of the maximum on the MEP. Figure 4 shows the breaking of the C−H bond, the forming of the O−H bond, and the change in distance between the C and O atoms along the MEP. Outside the range $s = \pm 0.5$ au the reactive bond distance changes in a concerted fashion with the C−O distance; thus the reactant species are moving together and product species are moving apart. On the product side of the MEP a change of the slope in r(C−H_a) and r(C−O) curves is observed due to the complex formation.

The force constant matrix was computed in steps of 0.2 au along the minimum energy path.[41] The resulting generalized normal modes were reordered by projecting the eigenvectors of successive steps onto each other, and connecting the ones giving the largest contribution for a specific eigenvector. Due to the strong mixing of frequencies, the reordering and connection of frequencies were not completely straightforward and some chemical intuition was needed to connect the frequencies reasonably. As can be seen in Figure 5, the generalized normal modes change mostly from $s = -1.0$ to $s = +1.0$ on the minimum energy path. Further on the path changes are smaller and can be easily interpolated over longer distance. Therefore, the forces were calculated up to $s = 1.5$ au for fluoroethane and chloroethane reactions with OH radical. For the ethane reaction with OH radical MEP was calculated up to $s = +0.8$ au due to convergence problems of the IRC algorithm, and consequently forces are calculated up to this point.

Out of all $3N - 7$ generalized normal modes there are only two that change significantly during the reaction (see Figure

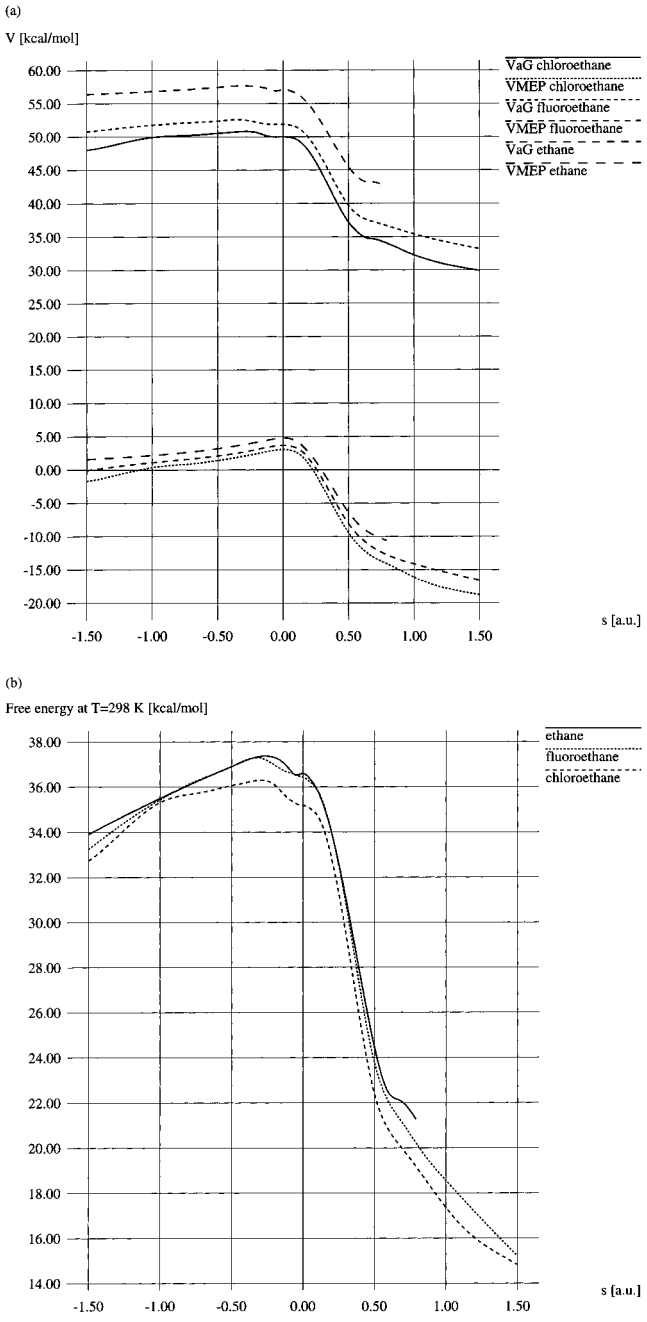

Figure 3. (a) Born−Oppenheimer potential energy (V_{MEP}), vibrationally adiabatic ground-state potential energy (V_a^G), and (b) the free energy at 298 K along the reaction path for reactions R1, R2, and R3.

5). These are the symmetric C−H stretching of the CH_2 group from which hydrogen is abstracted and the symmetric O−H stretching in the product water molecule. In the beginning of the reaction path its direction corresponds to the translational motion of the reactant units changing to symmetric C−H stretching at about $s = -1.0$ au. Toward the products this mode changes to the H−C−C bending mode on the resulting hydrocarbon radical. On the product side of the MEP, the direction of reaction path correspond to the symmetric O−H stretching frequency in water. This frequency changes continuously from the rocking of the CH_2 group, on the reactant side of the path, to the symmetric O−H mode of the product water molecule. At $s > 1.0$ au the direction of the reaction path becomes a translational motion toward the van der Waals complex structure and finally toward the separate product molecules. At the transition state the direction of the reaction path corresponds to the coupling of C−H_a and O−H_a stretching modes, i.e., transfer of hydrogen from ethane or haloethane to

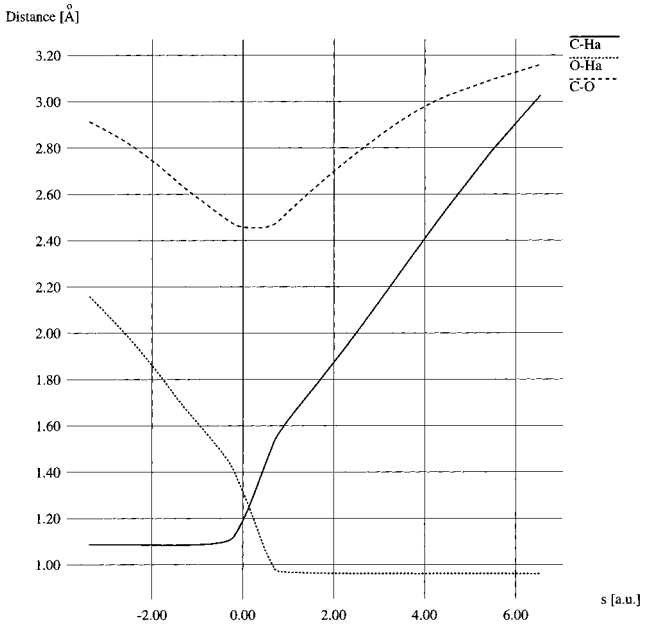

Figure 4. Change of reactive geometrical parameters r(C−H_a) and r(O−H_a) and the change of distance between C and O atoms along the minimum energy path for the fluoroethane reaction with hydroxyl radical.

the OH radical. Stretching of the O−H bond in the reactant hydroxyl radical molecule changes to antisymmetric O−H stretching in water. This frequency stays almost constant along the MEP. Also, bending of the CH_2 group in the reactant molecule changes to the slightly higher frequency of H−O−H bending in water molecule. Changes in the nonadiabatic coupling constants $B_{F,k}$ ($k = 1, 6, 11, 12$) with respect to s are displayed in Figure 6 for the reaction of fluoroethane with OH radical. The ν_1, ν_{11}, and ν_{12} modes show significant coupling to the reaction path. A large coupling of modes ν_1 and ν_{11} with the reaction path suggests that their excitation would accelerate the reaction.[32b,d−f] Similar conclusions can be drawn for ethane and chloroethane reactions with OH radical.

For all three reactions the two lowest frequency modes of the generalized transition state become imaginary along the MEP. As discussed elsewhere[9b] this may occur because potential-energy surface is not highly accurate or the MEP following algorithm is not fully converged or because of the unphysical nature of the Cartesian coordinate system. Therefore, we interpolated those generalized transition-state frequencies directly from the frequencies at the transition state, reactants and products in terms of the IVTST-0 treatment.[9b]

The consequence of the frequencies change along the MEP for the adiabatic ground-state potential energy is shown on Figure 3a. The maximum of the ground-state vibrationally adiabatic potential energy curve appears at $s_*^{AG} = -0.29$ au for reaction R1, $s_*^{AG} = -0.34$ au for reaction R2, and $s_*^{AG} = -0.29$ au for reaction R3. The shift of maxima toward reactants is due to the strong change of the $\nu(CH_2)$ mode on the reactant side of the MEP which is not compensated with lowering of potential energy since reaction path is relatively flat in this region. On the product side the MEP is much steeper and the change in potential energy along the reaction path is larger than the change in zero-point energy. The canonical variational dividing surface (the maximum of the free energy curve) is obtained at $s_*^{CVT} = -0.26$ au, $s_*^{CVT} = -0.33$ au, and $s_*^{CVT} = -0.29$ au at 298 K, for ethane, fluoroethane, and chloroethane reaction with hydroxyl radical (Figure 3b). This illustrates the competition between potential energy and vibrational energy in determining the location of the variational transition state. A much smaller effect of optimizing the dynamical bottleneck was

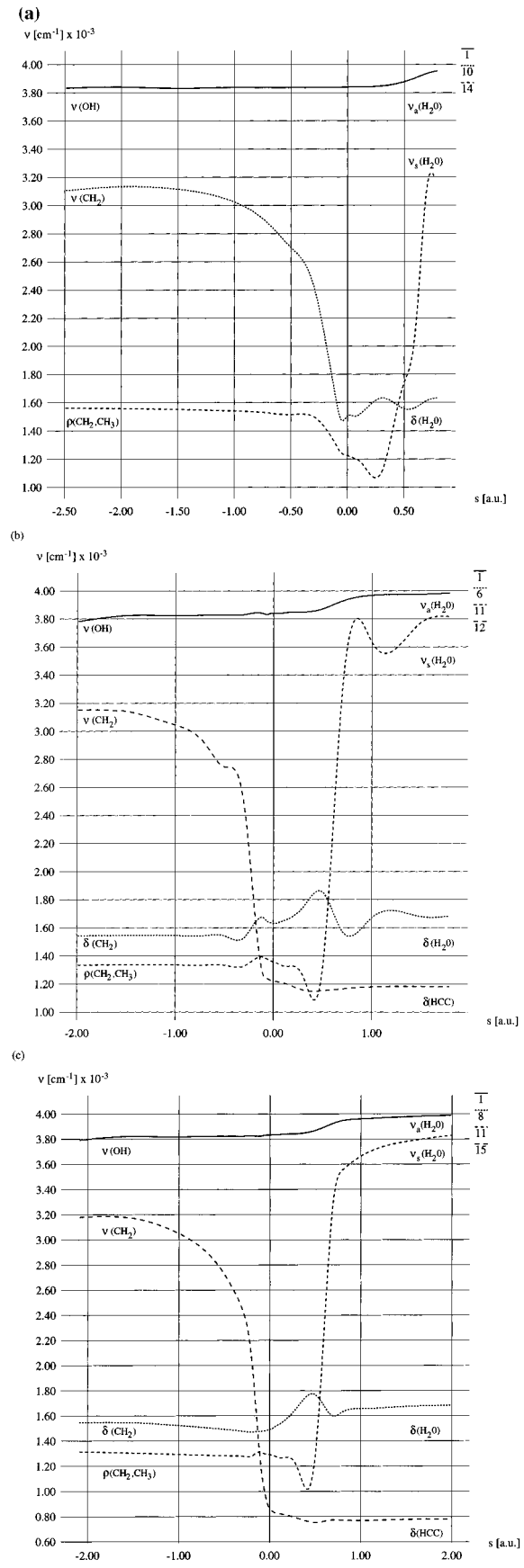

Figure 5. Selected generalized normal modes and their change along the minimum energy path for (a) ethane, (b) fluoroethane, and (c) chloroethane reactions with hydroxyl radical.

found in the previous studies[6c] with shifts to the product side. The difference coming from the fact that the reaction rate constants were calculated using the zero-order IVTST with one extra point calculated at 0.005 au. The reactant side of the MEP

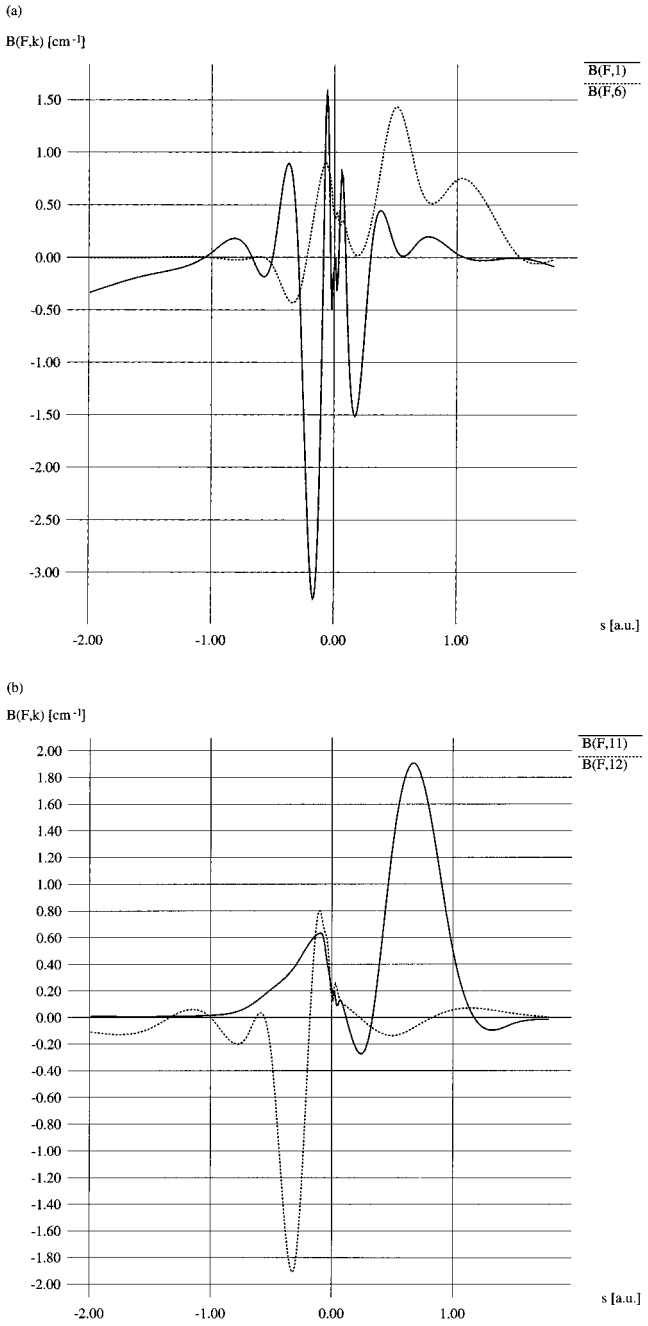

Figure 6. Changes of the nonadiabatic coupling constants $B(F,k)$ along the minimum energy path for the fluoroethane reaction with hydroxyl radical.

was not investigated and the significant changes in the vibrational frequencies have not been noticed.

There are two hindered rotations in the transition-state structures for all three reactions; internal rotation of hydroxyl group around the reactive O−H_a bond and internal rotation around the C−C bond. The rotation of the C−C bond was treated harmonically in all cases since treating this mode as a hindered rotor decreases the partition functions only 1% up to 3000 K. Frequencies for this torsional motion calculated at MP2/6-31G(d,p) level are 181, 260, and 263 cm^{-1} for the ethane, fluoroethane, and chloroethane transition-state structures, respectively. Frequencies for the internal rotations of the O−H group in the transition-state structures are 57, 228, and 153 cm^{-1}. The calculated rotational barriers are 0.08, 1.00, and 0.34 kcal mol^{-1} for the ethane, fluoroethane, and chloroethane transition-state structures, respectively. For the reaction of ethane with OH radical, the anharmonic treatment of this internal rotation decreases the reaction rate constants by 2% at room temperature,

6% at 1000 K, 13% at 2000 K, and 18% at 3000 K. For reactions R2 and R3 differences are negligible, both in the partition functions and in the reaction rate constants, since corresponding frequencies for these internal rotations are much higher than in the case of the ethane transition-state structure.

The reduced moment of inertia for the internal rotations of the O−H group in the transition-state structure is calculated for ethane reaction as a rotation of OH group about the O···H_a bond with 2-fold sinusoidal barrier. The same procedure is applied for the fluorethane and chloroethane reactions using the symmetry number equal to one. The calculated reduced moments of inertia are 1.9×10^{-47} kg m^2 for ethane, 6.7×10^{-47} for fluoroethane, and 8.6×10^{-47} for chloroethane transition-state structures. Our calculated value for ethane reaction is in a good agreement with the previously published value[7a] of 1.4×10^{-47} kg m^2. Truhlar et al.[6c] have treated this internal rotation in ethane reaction as a large-amplitude rotation of the ethyl group around the reactive C···H_a bond. Thus, their calculated reduced moment of inertia is 2.8×10^{-46} kg m^2, an order of magnitude larger than the above values.

Reaction Rate Constants. The interpolated variational transition-state theory based on the minimum energy path and its first and second derivatives calculated at the MP2/6-31G-(d,p) level of theory was used to calculate the reaction rate constants for ethane, fluoroethane, and chloroethane reactions with hydroxyl radical. This approach was improved by interpolated corrections of the barrier height at G2(MP2) level of theory. A complete notation for this dual-level dynamic approach will be G2(MP2)///MP2/6-31G(d,p) but, for practical reasons, the reaction rate constants calculated by this approach will be noted in the following text only as k^{CVT}.

Total reaction rate constants were calculated as a product of two different factors, the contribution from k^{CVT} which corresponds to the classical reaction-coordinate motion and the correction for tunneling, κ. Tunneling was estimated using the zero-curvature and small-curvature approximations. The temperature dependence of the calculated reaction rate constants for ethane, fluoroethane, and chloroethane reactions with OH radical is shown in Figure 7. It can be seen that the reaction rate constants are underestimated by variational and conventional approaches for all three reactions. The best agreement with experimental results is obtained for conventional transition state theory with Wigner tunneling correction. This agreement is most probably due to the fortuitous cancellation of errors, i.e., the overestimation of the barrier height by the conventional transition-state theory is offset by the Wigner's empirical overestimation of the tunneling effect. The canonical variational transition state rates are somewhat smaller than conventional since the maximum of the adiabatic ground-state potential is shifted from the $s = 0$ for all three reactions as described earlier. The difference between TST and CVT values is a measure of how much recrossing occurs for the conventional transition state. Variational optimization of the transition state location reduces the rate constants for ethane by 4%, for fluoroethane by 4.5%, and for chloroethane by 5.4% at 300 K. This lowering is larger at lower temperatures.

The transmission coefficients (κ) were calculated using the semiclassical zero-curvature (ZCT) and small-curvature (SCT) tunneling approximations. At room temperature κ^{SCT} is 2.37 for ethane, 2.04 for fluoroethane, and 2.07 for chloroethane reaction with OH radical. κ^{SCT} is about 20% larger than κ^{ZCT} at room temperature for all three reactions studied. The differences between two approaches become smaller at higher temperatures and negligible for temperatures over 1000 K.

The differences between the CVT/SCT results and experimental data are probably due to two potential sources of errors.

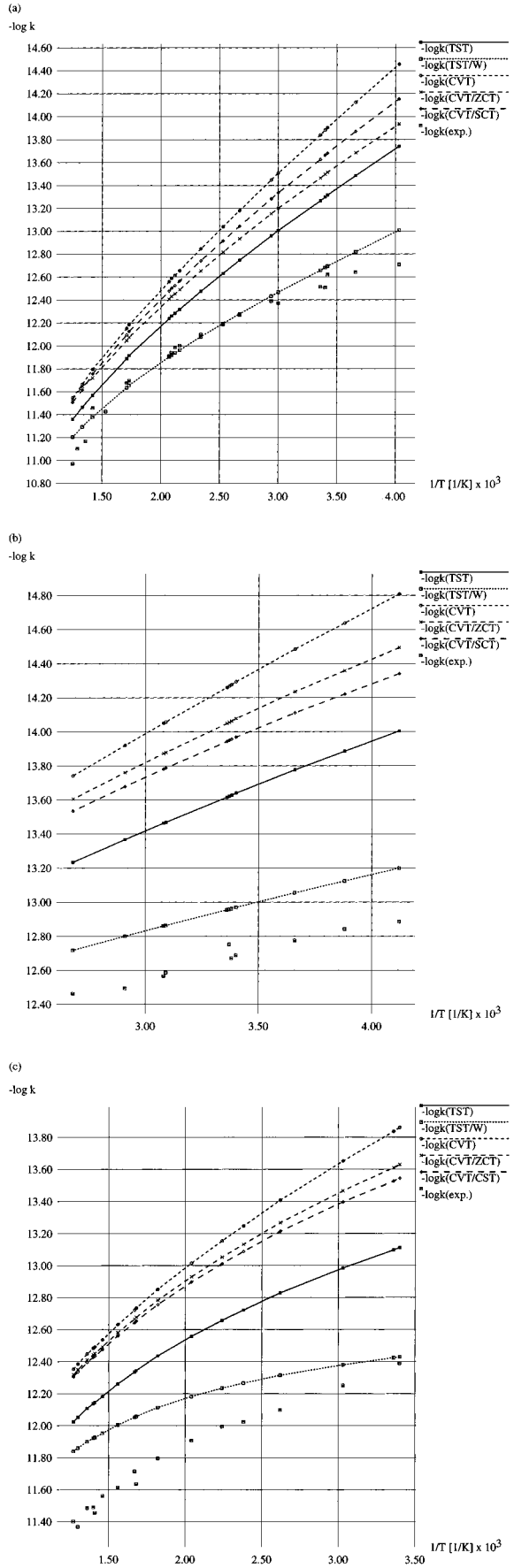

Figure 7. Temperature dependence of the experimental and calculated reaction rate constants for (a) ethane, (b) fluoroethane, and (c) chloroethane reactions with hydroxyl radical. The reaction rate constants have been calculated at the G2(MP2)///MP2/6-31G(d,p) level of theory using the conventional (TST) and canonical (CVT) transition-state theory with the Wigner (W), zero-curvature (ZCT), and small-curvature (SCT) tunneling corrections.

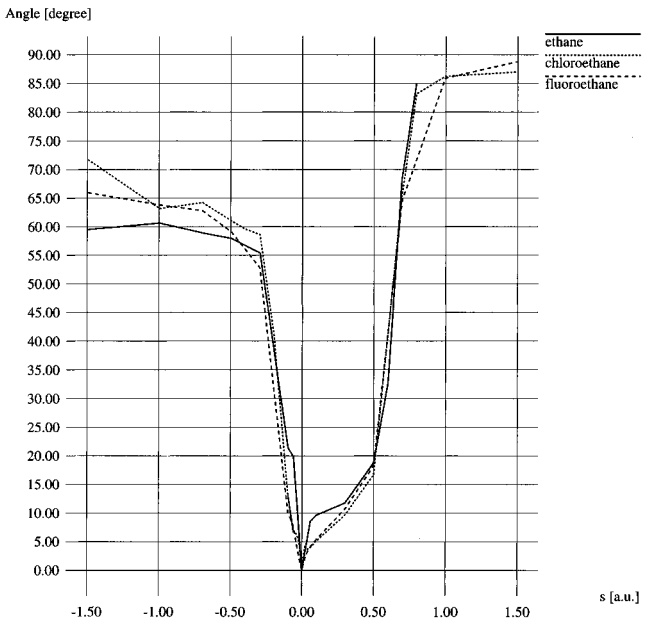

Figure 8. Change of angles between the gradient along the minimum energy path and the imaginary-frequency normal mode eigenvector at the transition state for reactions R1, R2, and R3.

One is the use of small-curvature (SCT) tunneling approximation which is known[30,42,43] to underestimate the tunneling contribution for reactions in which a light atom is transferred between two heavy moieties. Thus, the tunneling effect is not properly accounted for and this is most probably the largest source of error in the calculated reaction rate constants at low temperatures. (Note the larger discrepancies between the experimental and calculated reaction rate constants at lower temperatures.) The other source of discrepancies between experimental and calculated rate constants is the accuracy of the MEP and the first and second derivatives calculated on the MEP. In our IVTST-IC approach we have corrected only the classical barrier heights with respect to the energies calculated at G2(MP2) level, using the frequencies and inertia tensors from the low-level MP2/6-31G(d,p) calculations. Thus, more accurate frequencies would be desirable for the interpolated corrections too. Finally, the effect of anharmonicity is not included in this study. Its inclusion was found[44] to lower the thermal rate constants for hydrogen abstraction from methane by a hydrogen atom. A similar effect may be expected for reactions investigated in this work.

The validity of the SCT approximation can be tested by considering the angle between the imaginary-frequency normal-mode eigenvector at the transition state and the gradient along the MEP. Figure 8 displays this angle calculated for all three reactions showing a very similar pattern and therefore implying a similar reaction mechanism. Angles between the MEP and imaginary frequency eigenvector change very rapidly up to −0.3 au, where the maximum of the adiabatic ground-state potential energy curve occurs, and up to 1.0 au on the product side of the MEP. Outside this range they are relatively constant. This angle represents approximately the amount that the MEP has curved away from a straight line due to the coupling with vibrational modes (Figure 8). The turning points at the representative SCT tunneling energies[28] are calculated to be at −0.71 and −0.10 au for reaction R1, at −0.66 and −0.18 au for reaction R2, and at −0.57 and −0.20 au for reaction R3. It can be seen from Figure 8 that the angles are fairly large in the representative tunneling region.

It would be interesting to estimate the contribution from the large curvature tunneling approximation. At present, the large curvature tunneling (LCT) calculations[13,25,42,45] are available only within direct dynamics approaches where one has to use the semiempirical molecular orbital calculations to keep the calculations computationally feasible.[9b] To produce a reasonable MEP, semiempirical calculations have to be parametrized specifically for the reaction of interest.[6d,9b,10] At the same time correct structures and frequencies are needed, which is a quite difficult task.[9b,10] It is generally known[6d,9b,11,23c,26,42,43] that semiempirical methods without adjustment of the parameters are not suitable for direct dynamics calculations. Further extensive work is needed to optimize specific reaction parameters for the hydrogen abstraction reactions in order to estimate the large curvature tunneling transmission coefficients.

TABLE 3: Comparison of Activation Entropies ($\Delta^{\ddagger}S^{\circ}$) Obtained from Experimentally Determined Preexponential Factors and Calculated by ab Initio Methods at 298 K and Reported in cal mol^{-1} K^{-1}[a]

reaction	10^{-12}A	$\Delta^{\ddagger}S^{\circ}$(exp)[e]	$\Delta^{\ddagger}S^{\circ}$(exp)[f]	$\Delta^{\ddagger}S^{\circ}$(calc)[f]
C_2H_6 + OH	10.3[b]	−112.9	−24.1	−22.1
C_2H_5F + OH	6.7[c]	−115.5	−25.0	−28.4
C_2H_5Cl + OH	14.0[d]		−23.4	−27.7

[a] The preexponential factors (A), in cm^3 molecule^{-1} s^{-1}, are obtained from the experimental reaction rate constants. [b] References 1 and 35. [c] Reference 36. [d] Reference 37. [e] Reference 7b. [f] This work.

It was suggested earlier[7b] that tunneling must be significant in the reactions of hydroxyl radical with fluorinated ethanes. It was found, in that study, that the activation entropies calculated by ab initio methods are 4 times smaller than the values obtained from experimentally determined preexponential factors. Thus, it was concluded that the reason for such large discrepancies between calculated and "experimental" activation entropies must be the curvature in the Arrhenius plot as a result of tunneling. We have recalculated both activation entropies for all three reactions from this study. Results of both studies are presented in Table 3 while the procedure that we used to derive "experimental" activation entropies is described in ref 46. Our results show, in contrast to previous findings,[7b] that the differences between experimental and theoretical values are quite small, up to 4 cal K^{-1} mol^{-1}. It seems to us that the reason for such large discrepancies between "experimental" activation entropies determined in these two studies (Table 3, columns 2 and 3) is an inadequate procedure used in a previous study[7b] to obtain "experimental" activation entropies. More specifically, the difference between the thermodynamic equilibrium constant (K°) and the equilibrium constant for perfect gas mixture expressed in terms of the concentrations of the species at equilibrium (K_c)[46] must have been overlooked. Thus, it is fair to conclude that the differences between theoretical and experimental activation entropies (Table 3, columns 3 and 4) are quite small for all three reactions and can be explained by errors in calculated and experimental values.

Since the understanding of substituent effects is very important in the atmospheric chemistry of haloalkanes, we have compared results for ethane reaction with hydroxyl radical with fluoroethane and chloroethane reactions in order to understand the effect of halogen substitution. In our previous work[8b] we have discussed electronic factors affecting barrier heights of ethane and its halogenated analogues. However, Truhlar et al.[6c] have shown that the explanation of substituent effects based only on the electronic factors affecting the barrier heights cannot account qualitatively for the whole effect. Therefore, we have factorized the rate constant ratios into the tunneling (TunF), symmetry (SymmF), rotational (RotF), translational (TranF), vibrational (VibF), and potential (PotF) contributions. Table 4 lists these contributions calculated at TST and CVT/SCT levels and for three different temperatures 300, 600, and 1000 K for $k_{(FEt)}/k_{(C_2H_6)}$ and $k_{(ClEt)}/k_{(C_2H_6)}$ ratios.

TABLE 4: Reaction Rate Constants Ratios Factorized[a] into the Tunneling (TunF), Symmetry (SymmF), Rotational (RotF), Translational (TranF), Vibrational (VibF), and Potential (PotF) Contributions

method	*T* (*K*)	TunF	SymmF	TranF	RotF	VibF	PotF	k_{HalEt}/k_{Et}
				Chloroethane				
TST	300		0.333	0.727	0.326	0.981	19.05	1.48
	600		0.333	0.727	0.326	0.951	4.32	0.33
	1000		0.333	0.727	0.326	0.945	2.41	0.18
CVT/SCT	300	0.859	0.333	0.727	0.326	0.588	21.57	0.87
	600	0.952	0.333	0.727	0.325	0.589	5.02	0.22
	1000	0.981	0.333	0.727	0.325	0.607	2.78	0.14
				Fluoroethane				
TST	300		0.333	0.804	0.756	0.333	6.63	0.45
	600		0.333	0.804	0.756	0.412	2.56	0.21
	1000		0.333	0.804	0.756	0.444	1.76	0.16
CVT/SCT	300	0.874	0.333	0.804	0.754	0.195	9.63	0.33
	600	0.957	0.333	0.804	0.755	0.273	3.27	0.18
	1000	0.983	0.333	0.804	0.756	0.319	2.07	0.13

[a] The factorization procedure is performed for results obtained with the conventional (TST) and variational (CVT/SCT) transition-state theory at three different temperatures.

At all temperatures examined, PotF favors reactions R2 and R3 over reaction R1. However, other factors lower this contribution significantly resulting in smaller $k_{(HalEt)}/k_{(Et)}$ ratios. PotF decreases with increasing the temperature while TunF and VibF increase. In the case of fluoroethane, increase of VibF with the temperature is more pronounced than in the case of chloroethane. It should be noted that TST and CVT ratios differ significantly for VibF contributions. This is the consequence of larger variational effects on the position of the dynamical bottleneck in the case of haloethanes resulting in significantly different VibF factors. At the 300 K TST $k_{(ClEt)}/k_{(C_2H_6)}$ ratio is 1.48, while the CVT/SCT ratio is only 0.87. Results obtained with the conventional transition-state theory are closer to the experimental ratio, but it must be noted that the experimental results for chloroethane and fluoroethane cannot be compared directly with calculated values of the reaction rate constants since the experimental reaction rate constants have been determined for overall abstraction process, i.e., the abstraction reactions from both α- and β-carbon atoms, while the calculated reaction rate constants apply only for α abstraction.

Conclusions

The present study provides a detailed description of the reaction-path dynamics of ethane, fluoroethane, and chloroethane reactions with OH radical. Three hydrogen abstraction reactions have been studied with canonical variational transition-state theory augmented with multidimensional semiclassical tunneling approximations. The minimum energy path and its first and second derivatives were calculated at the MP2(full)/6-31G(d,p) level of theory. This approach was supplemented by interpolated corrections of barrier heights calculated by G2(MP2) methodology.

The reaction rate constants of all three reactions have been calculated for temperatures from 200 to 1000 K which covers the range of experimentally determined values. The comparison of CVT and CVT/ZCT results has shown that tunneling is important for those hydrogen abstraction reactions and increases the reaction rate constants by a factor of 5 at 200 K and by a factor of 2 at 320 K. This temperature range is of particular interest for tropospheric reactions. The calculated reaction rate constants are smaller than the measured values for the whole temperature range, and the differences are more pronounced at low temperatures. However, if the measured values would be available specifically for the abstraction reactions from the α-carbon atom, the agreement with the calculated reaction rate constants of haloethanes would be improved.

The analysis of the reaction path properties has shown that two normal modes change significantly during the abstraction reactions. These are the symmetric C−H stretching of the CH_2 group from which hydrogen is abstracted and the symmetric O−H stretching in the product water molecule. The change of frequencies along the reaction path has a significant effect on the position of dynamical bottleneck for all three reactions. The competition between potential and vibrational energies in determining the location of the variational transition state shifts the dynamical bottleneck toward reactants.

Although the present study provides a detailed description of the reaction-path dynamics of important tropospheric reactions, to obtain more accurately calculated reaction rate constants the application of the higher level of theory for minimum energy path calculations and/or the large curvature tunneling corrections will be necessary. Both tasks are computationally demanding and time-consuming, however, we plan to pursue these research tasks in the future.

Acknowledgment. This work was supported by Grant 1-07-159 awarded by the Ministry of Science and Technology of the Republic of Croatia, by the U.S.−Croatian Science and Technology Joint Fund in cooperation with U.S. Department of Agriculture and Croatian Ministry of Science and Technology under Project Number JF-120, and by the Forschungsförderungsfonds of Austria under Project Number P10404-PHY. This work was also carried out under the framework of the project "Fate and Activity Modeling of Environmental Pollutants using Structure−Activity Relationships (FAME)", financially supported by the Environment and Climate Research and Technological Development Program of the Commission of the European Union under Contract ENV4-CT96-0211 (DG 12-ESCY). Financial support from the European Union is gratefully acknowledged. Authors are also grateful to Professor T. Cvitaš for fruitful discussion.

References and Notes

(1) (a) Atkinson, R. *Chem. Rev. (Washington, D.C.)* **1986**, *86*, 69. (b) Atkinson, R. *J. Phys. Chem. Ref. Data* **1989**, Monograph 1. (c) Atkinson, R.; Baulch, D. L.; Cox, R. A.; Hampson, R. F., Jr.; Kerr, J. A.; Troe, J. *J. Phys. Chem. Ref. Data* **1989**, *18*, 881. (d) Atkinson, R. *J. Phys. Chem. Ref. Data* **1994**, Monograph 2.

(2) (a) Stolarski, R.; Bojkov, R.; Bishop, L.; Zerefos, C.; Staehelin, J.; Zawodny, J. *Science* **1992**, *256*, 342. (b) Kerr, R. A. *Science* **1993**, *262*, 501. (c) Kerr, J. B.; McElroy, C. T. *Science* **1993**, *262*, 1032. (d) Newman, A. *Environ. Sci. Technol.* **1993**, *27*, 1488. (e) Ravishankara, A. R.; Turnipseed, A. A.; Jensen, N. R.; Barone, S.; Mills, M.; Howard, C. J.; Solomon, S. *Science* **1994**, *263*, 71. (f) Schwarzbach, S. E. *Nature* **1995**, *376*, 297.

(3) *Progress and problems in atmospheric chemistry*: Advanced Series in Physical Chemistry; Barker, J. R., Ed.; World Scientific Publishing Co.: Singapore; Vol. 3.

(4) (a) Manzer, L. *Science* **1990**, *249*, 31. (b) Solomon, S. *Nature* **1990**, *347*, 6291. (c) Freemantle, M. *Chem. Eng. News* **1994**, *72*, 2 (No. 38), 29. (d) Schwarzbach, S. E. *Nature* **1995**, *376*, 297.

(5) (a) Dorigo A. E.; Houk, K. N. *J. Org. Chem.* **1988**, *53*, 1650. (b) Truong, T. N.; Truhlar, D. G. *J. Chem. Phys.* **1990**, *93*, 1761. (c) Gonzales, C.; McDouall, J. J. W.; Schlegel, H. B. *J. Phys. Chem.* **1990**, *94*, 7467. (d) Lasaga, A. C.; Gibbs, G. V. *Geophys. Res. Lett.* **1991**, *18*, 1217. (e) Dobbs, K. D.; Dixon, D. A.; Komornicki, A. *J. Chem. Phys.* **1993**, *98*, 8852. (f) Francisco, J. S. *J. Chem. Phys.* **1992**, *96*, 7597. (g) Francisco, J. S. *J. Chem. Soc., Faraday Trans.* **1992**, *88*, 1943. (h) McKee, M. L. *J. Phys. Chem.* **1993**, *97*, 10971. (i) Rayez, M.-T.; Rayez, J.-C.; Berces, T.; Lendvay, G. *J. Phys. Chem.* **1993**, *97*, 5570. (j) Bottoni, A.; Poggi, G.; Emmi, S. S. *J. Mol. Struct. (THEOCHEM)* **1993**, *279*, 229. (k) Walch, S. P. *J. Chem. Phys.* **1993**, *98*, 3163. (m) Fu, Y. J.; Lewisbevan, W.; Tirrell J. *J. Phys. Chem.* **1995**, *99*, 630.

(6) (a) Melissas, V. S.; Truhlar, D. G. *J. Chem. Phys.* **1993**, *98*, 1013. (b) Melissas, V. S.; Truhlar D. G. *J. Chem. Phys.* **1993**, *99*, 3542. (c) Melissas, V. S.; Truhlar, D. G. *J. Phys. Chem.* **1994**, *98*, 875. (d) Corchado, J. C.; Espinosa-Garcia, J.; Hu, W.-P.; Rossi, I.; Truhlar, D. G. *J. Phys. Chem.* **1995**, *99*, 687.

(7) (a) Martell, J. M.; Mehta, A. K.; Pacey, P. D.; Boyd, R. J. *J. Phys. Chem.* **1995**, *99*, 8661. (b) Martell, J. M.; Boyd, R. J. *J. Phys. Chem.* **1995**, *99*, 13402.

(8) (a) Sekušak, S.; Güsten, H.; Sabljić, A. *J. Chem. Phys.* **1995**, *102*, 7504. (b) Sekušak, S.; Güsten, H.; Sabljić, A. *J. Phys. Chem.* **1996**, *100*, 6212. (c) Sekušak, S.; Güsten, H.; Sabljić, A. *J. Phys. Chem. A* **1997**, *101*, 967 (correction). (d) Sekušak, S.; Sabljić, A. *J. Comput. Chem.*, in press.

(9) (a) Gonzalez-Lafont, A.; Truong, T. N.; Truhlar, D. G. *J. Chem. Phys.* **1991**, *95*, 8875. (b) Hu, W.-P.; Liu, Y.-P.; Truhlar, D. G. *J. Chem. Soc., Faraday. Trans.* **1994**, *90*, 1715.

(10) Liu, Y.-P.; Lynch, G. C.; Truong, T. N.; Lu, D.-h.; Truhlar, D. G.; Garrett, B. C. *J. Am. Chem. Soc.* **1993**, *115*, 2408.

(11) Truhlar, D. G. In *The Reaction Path in Chemistry: Current Approaches and Perspectives*; Heidrich, D., Ed.; Kluwer: Dordrecht, 1995; p 229.

(12) Truhlar, D. G.; Garrett, B. C. *Acc. Chem. Res* **1980**, *13*, 440.

(13) Truhlar, D. G.; Isaacson, A. D.; Garrett, B. C. In *Theory of Chemical Reaction Dynamics*; Baer, M., Ed.; CRC Press: Boca Raton, FL, 1985; Vol. 4, p 65.

(14) Møller, C.; Plesset, M. S. *Phys. Rev.* **1934**, *46*, 618.

(15) Hariharan, P. C.; Pople, J. A. *Chem. Phys. Lett.* **1972**, *66*, 217.

(16) Gonzalez, C.; Schlegel, H. B. *J. Phys. Chem.* **1990**, *94*, 5523.

(17) Curtiss, L. A.; Raghavachari, K.; Pople, J. A. *J. Chem. Phys.* **1993**, *98*, 1293.

(18) (a) Pople, J. A.; Head-Gordon, M.; Fox, D. J.; Raghavachari, K.; Curtiss, L. A. *J. Chem. Phys.* **1989**, *90*, 5622. (b) Curtiss, L. A.; Raghavachari, K.; Trucks, G. W.; Pople, J. A. *J. Chem. Phys.* **1991**, *94*, 7221.

(19) Schlegel, H. B. *J. Phys. Chem.* **1988**, *92*, 3075.

(20) (a) Frisch, A. M. J.; Trucks, G. W.; Head-Gordon, M.; Gill, P. M. W.; Wong, M. W.; Foresman, J. B.; Johnson, G. B.; Schlegel, H. B.; Robb, M. A.; Replogle, E. S.; Gomperts, R.; Anders, J. L.; Raghavachari, K.; Binkley, J. S.; Gonzalez, C.; Martin, R. L.; Fox, D. J.; Defrees, D. J.; Baker, J.; Stewart, J. J. P.; Pople, J. A. *Gaussian92*; Gaussian Inc.: Pittsburgh, PA, 1992. (b) Frisch, A. M. J.; Trucks, G. W.; Schlegel, H. B.; Gill, P. M. W.; Johnson, B. G.; Robb, M. A.; Cheesman, J. R.; Keith, T. A.; Petersson, G. A.; Montgomery, J. A.; Raghavachari, K.; Al-Laham, M. A.; Zakrzewski, V.G.; Ortiz, J. V.; Foresman, J. B.; Cioslowski, J.; Stefanov, B. B.; Nanayakkara, A.; Challacombe, M.; Peng, C. Y.; Ayala, P. Y.; Chen, W.; Wong, M. W.; Andres, J. L.; Replogle, E. S.; Gomperts, R.; Martin, R. L.; Fox, D. J.; Binkley, J. S.; Defrees, D. J.; Baker, J.; Stewart, J. P.; Head-Gordon, M.; Gonzalez, C.; Pople, J. A. *Gaussian 94, Revision C.2.* Gaussian, Inc., Pittsburgh PA, 1995.

(21) (a) Glasstone, S.; Laidler, K.; Eyring, H. *The Theory of Rate Processes;* McGraw-Hill: New York, 1941. (b) Moore, J.; Pearson, R. G. *Kinetics and Mechanism*, 3rd ed.; Wiley: New York, 1981.

(22) (a) Tucker, S. C.; Truhlar, D. G. *New Theoretical Concepts for Understanding Organic Reactions*; Bertran, J., Csizmadia, I. G., Eds; Kluwer: Dordrecht, The Netherlands, 1989; p 291. (b) Kreevoy, M. M.; Truhlar, D. G. *Investigation of Rates and Mechanisms of Reactions*, 4th ed.; Bernasconi, C. F., Ed.; Wiley: New York, 1986; Part 1, p 13.

(23) (a) Garrett, B. C.; Truhlar, D. G. *J. Am. Chem. Soc.* **1979**, *101*, 4534, 5207. (b) Truhlar, D. G.; Garrett, B. C. *Annu. Rev. Phys. Chem.* **1984**, *35*, 159. (c) Truhlar, D. G.; Garrett, B. C.; Klippenstein, S. J. *J. Phys. Chem.* **1996**, *100*, 12771.

(24) (a) Eliason, M. A.; Hirschfelder, J. O. *J. Chem. Phys.* **1959**, *30*, 1426. (b) Garrett, B. C.; Truhlar, D. G. *J. Chem. Phys.* **1979**, *70*, 1593. (c) Garrett, B. C.; Truhlar, D. G. *J. Phys. Chem.* **1979**, *83*, 1052, 1079; **1983**, *87*, 4553.

(25) (a) Steckler, R.; Hu, W.-P.; Liu, Y.-P.; Lynch, G. C.; Garrett, B. C.; Isaacson, A. D.; Lu, D.-H.; Melissas, V. S.; Truong, T. N.; Rai, S. N.; Hancock, G. C.; Lauderdale, J. G.; Joseph, T.; Truhlar, D. G. *POLYRATE-version 6.5*; University of Minnesota, Minneapolis, 1995. (b) Lu, D.-h.; Truong, T. N.; Melissas, V. S.; Lynch, G. C.; Liu, Y.-P.; Garrett, B. C.; Steckler, R.; Isaacson, A. D.; Rai, S. N.; Hancock, G. C.; Lauderdale, J. G.; Joseph, T.; Truhlar, D. G. *Comput. Phys. Commun.* **1992**, *71*, 235.

(26) Liedl, K. R.; Sekušak, S.; Kroemer, R. T.; Rode, B. M. *J. Phys. Chem. A*, in press.

(27) Truhlar D. G. *J. Comput. Chem.* **1990**, *12*, 266.

(28) Truhlar, D. G.; Kupperman, A. *J. Am. Chem. Soc.* **1971**, *93*, 1840.

(29) Truhlar, D. G.; Isaacson, A. D.; Skodje, R. T.; Garrett, B. C. *J. Phys. Chem.* **1982**, *86*, 2252.

(30) Skodje, R. T.; Truhlar, D. G.; Garrett, B. C. *J. Phys. Chem.* **1981**, *85*, 3019.

(31) Wigner, E. P. *Z. Phys. Chem. Abt. B* **1932**, *19*, 203.

(32) (a) Truong, T. N. J. *Chem. Phys.* **1994**, *100*, 8014. (b) Bell, R. L.; Truong, T. N. *J. Chem. Phys.* **1994**, *101*, 10442. (c) Duncan, W. T.; Truong, T. N. *J. Chem. Phys.* **1995**, *103*, 9642. (d) Hofacker, G. L.; Michel, K. W. *Ber. Bunsen-Ges. Phys. Chem.* **1974**, *78*, 174. (e) Duff, J. W.; Truhlar, D. G. *J. Chem. Phys.* **1975**, *62*, 2477. (f) Morokuma, K.; Sato, S. In *Potential Energy Surfaces and Dynamic Calculations;* Truhlar, D. G., Ed.; Plenum: New York, 1981; p 243.

(33) (a) Lu, D-h; Maurice, D.; Truhlar, D. G. *J. Am. Chem. Soc.* **1990**, *112*, 6205. (b) Liu, Y.-P.; Lynch, G. C.; Truong, T. N.; Lu, D.-h.; Truhlar, D. G.; Garrett, B. G. *J. Am. Chem. Soc.* **1993**, *115*, 2408. (c) Hu, W. P.; Truhlar, D. G. *J. Am. Chem. Soc.* **1996**, *118*, 860. (d) Allison, T. C.; Lynch, G. C.; Truhlar, D. G.; Gordon, M. S. *J. Phys. Chem.* **1996**, *100*, 13575.

(34) (a) Mielke, S. L.; Truhlar, G. C.; Schwenke, D. W. *J. Phys. Chem.* **1994**, *98*, 8000. (b) Mielke, S. L.; Allison, T. C.; Truhlar, D. G.; Schwenke, D. W. *J. Phys. Chem.* **1996**, *100*, 13588.

(35) (a) Sharkey, P.; Smith, I. W. M. *J. Chem. Soc., Faraday Trans.* **1993**, *89*, 631. (b) Taldukar, R. K.; Mellouki, A.; Gierczak, T.; Barone, S.; Chiang, S.-Y.; Ravishankara, A. R. *Int. J. Chem. Kinet.* **1994,** *26*, 973.

(36) (a) Schmoltner, A. M.; Talukdar, R. K.; Warren, R. F.; Mellouki, A.; Goldfarb, L.; Gierczak, T.; McKeen, S. A.; Ravishankara, A. R. *J. Phys. Chem.* **1993**, *97*, 8976. (b) Hsu, K.-J.; DeMore, W. B. *J. Phys. Chem.* **1995**, *99*, 1235.

(37) Kasner, J. H.; Taylor, P. H.; Dellinger, B. *J. Phys. Chem.* **1990**, *94*, 3250.

(38) Atkins, P. W. *Physical Chemistry*, 5th ed.; Oxford University Press: Oxford, 1994.

(39) Pacey, P. D. *J. Chem. Educ.* **1981**, 58, 613.

(40) (a) Foster, P.; Weinhold, F. *J. Am. Chem. Soc.* **1980**, *102*, 7211. (b) Reed, A. E.; Weinhold, F. *J. Chem. Phys.* **1983**, *78*, 4066. (c) Reed, A. E.; Weinstock, R. B.; Weinhold, F. *J. Chem. Phys.* **1985**, *83*, 735. (d) Reed, A. E.; Weinhold, F. *J. Chem. Phys* **1985**, *83*, 1736. (e) Reed, A. E.; Curtiss, L. A.; Weinhold, F. *Chem. Rev. (Washington, D.C.)* **1988**, *88*, 899. (f) Glendening, E. D.; Reed, A. E.; Carpenter, J. E.; Weinhold, F. *NBO program, Version 3.1*.

(41) Miller, W. H.; Handy, N. C.; Adams, J. E. *J. Chem. Phys.* **1980**, *72*, 99.

(42) Liu, L.-P.; Lu, D.-h; Gonzalez-Lafont, A.; Truhlar, D. G. *J. Am. Chem. Soc.* **1993**, *115*, 7806.

(43) Kim, Y. *J. Am. Chem. Soc.* **1996**, *118*, 1522.

(44) Joseph, T.; Garrett B. C.; Truhlar, D. G. *J. Chem. Phys.* **1988**, *88*, 6982.

(45) (a) Garrett, B. C.; Joseph, T.; Truong, T. N.; Truhlar, D. G. *Chem. Phys.* **1989**, *136*, 271.

(46) The Eyring equation for the reaction rate constant is $k = \kappa(kT/h) \times K_c$. The K_c is given by $K_c = (p^o/kT)^{1-\mu}K^o$, where μ is the molecularity of the reaction. Thus, the reaction rate constant is $k = (kT/h)(p^o/kT)^{1-\mu}e^{-\Delta^\ddagger G^o/RT} = (kT/h)(p^o/kT)^{1-\mu}e^{\Delta^\ddagger S^o/RT}e^{\mu}e^{-E_a/RT}$ since $\Delta^\ddagger H^o = E_a + \mu RT$ and E_a is Arrhenius activation energy. If this expression is equalized with Arrhenius equation the activation entropy values can easily be calculated from the preexponential factors. If the activation entropies are calculated without the factor $(p^o/kT)^{1-\mu}$, values from the ref 7b are obtained. For more detailed description see ref 38, p 941.